Disruption mitigation by injection of small quantities of noble gas in ASDEX Upgrade

2017 Plasma Phys. Control. Fusion 59 014046

(http://iopscience.iop.org/0741-3335/59/1/014046)

IOP Publishing Plasma Physics and Controlled Fusion

Plasma Phys. Control. Fusion **59** (2017) 014046 (11pp) doi:10.1088/0741-3335/59/1/014046

Disruption mitigation by injection of small quantities of noble gas in ASDEX Upgrade

G Pautasso[1], M Bernert[1], M Dibon[1], B Duval[2], R Dux[1], E Fable[1], J C Fuchs[1], G D Conway[1], L Giannone[1], A Gude[1], A Herrmann[1], M Hoelzl[1], P J McCarthy[3], A Mlynek[1], M Maraschek[1], E Nardon[4], G Papp[1], S Potzel[1], C Rapson[1], B Sieglin[1], W Suttrop[1], W Treutterer[1], The ASDEX Upgrade team[1] and The EUROfusion MST1 team[5]

[1] Max-Plank-Institute für Plasma Physik, D-85748 Garching, Germany
[2] Swiss Plasma Centre, EPFL, CH-1016 Lausanne, Switzerland
[3] Department of Physics, University College Cork, Cork, Ireland
[4] CEA, IRFM, F-13108 Saint Paul lez Durance, France

E-mail: gap@ipp.mpg.de

Received 11 July 2016, revised 13 October 2016
Accepted for publication 13 October 2016
Published 22 November 2016

Abstract

The most recent experiments of disruption mitigation by massive gas injection in ASDEX Upgrade have concentrated on small—relatively to the past—quantities of noble gas injected, and on the search for the minimum amount of gas necessary for the mitigation of the thermal loads on the divertor and for a significant reduction of the vertical force during the current quench. A scenario for the generation of a long-lived runaway electron beam has been established; this allows the study of runaway current dissipation by moderate quantities of argon injected. This paper presents these recent results and discusses them in the more general context of physical models and extrapolation, and of the open questions, relevant for the realization of the ITER disruption mitigation system.

Keywords: disruption mitigation, runaway electrons, MGI

(Some figures may appear in colour only in the online journal)

1. Introduction

The tokamak plasma can be subject to a major instability, called a disruption, which terminates the discharge [1]. Disruptions can damage machine components since they cause large mechanical forces in the conductive structures of the tokamak and large power loads onto the plasma facing components. Disruption studies address the identification of the causes leading to these instabilities, the simulation of their effects by means of physical models and the development of prediction algorithms and mitigation methods. In this way disruption studies complement fusion research activities aimed at the development and control of stable plasma scenarios.

A relatively simple but efficient method of mitigating a disruption in existing devices has been the injection of impurity material, mainly noble gas in the gaseous or frozen state, into the pre-disruptive plasma. The impurity atoms, assimilated by the plasma, radiate part of the thermal energy before it is conducted onto the divertor plates during the thermal quench (TQ). Moreover, the choice of the impurity type, quantity and injection scheme allows some control on the current quench (CQ) duration, indirectly on the magnitude of the mechanical forces, and on the runaway electron (RE) current generation and dissipation.

A disruption mitigation system (DMS) is also foreseen for the international experimental reactor ITER; this system is presently being designed and integrated into the overall plant system [2].

Extensive studies of disruption mitigation on the ASDEX Upgrade tokamak (AUG), using massive gas injection (MGI), have significantly contributed to the progress made in recent years in understanding the dynamics of the induced plasma shut-down (see [3] and references within). This understanding

[5] www.euro-fusionscipub.org/mst1

is a prerequisite for the formulation of appropriate mitigation schemes for ITER.

This article reports on the work of disruption mitigation—its motivation, experimental results and theoretical understanding—conducted on AUG in the last two years. The article consists of two main sections dedicated, firstly, to the mitigation of the TQ and of the mechanical forces (section 3) and, secondly, to the investigation of RE generation and suppression (section 4).

These most recent MGI experiments (section 3.1) have concentrated on small (relative to previous studies) quantities of noble gas injected, and particularly on the search for the minimum amount of gas necessary for the TQ mitigation. Parallel to the experimental work, the pre-thermal-quench (pre-TQ) phase, i.e. between the arrival of the gas at the plasma edge and the TQ, of different AUG MGI induced plasma termination scenarios has been simulated with the transport code ASTRA-STRAHL [4]. The code has been used to understand the experimentally observed dependence of the pre-TQ duration on the plasma and gas parameters (section 3.2).

In the experiment, the quantity of injected neon was decreased until the vertical force on the machine approached unmitigated values; the dependence of the current quench duration, of the vertical force and of the halo current magnitude on the neon quantity is reported in the following (section 3.3). Moreover, the influence of the quantity of injected impurities on the repartition between radiated and deposited power during the TQ is discussed (section 3.4). The toroidal asymmetry of the radiated power during the pre-TQ and its dependence on the valve position, with respect to the MHD mode position, has been documented (section 3.5).

Studies of RE generation and suppression are rather recent in AUG. After a description of the experimental scenario (section 4.2), this paper concentrate on the discussion of the RE current suppression by injection of moderate quantities of high-Z noble gases (section 4.3).

2. Background

Previous (2008–2013) experiments on AUG were aimed at injecting the amount of gas necessary to reach the so-called critical density, $n_c = \mathcal{O}(10^{22})$ m^{-3}, during or just after the TQ. This value of the density would in fact assure the RE suppression in a future ITER CQ, in spite of the expected large toroidal electric field. For this purpose, large quantities of neon atoms, i.e. $N_{inj} = 1 \times 10^{22}$–$20 \times 10^{22}$, were injected into AUG plasmas (with a volume of circa 13 m^3). Nevertheless, the assimilation of gas decreases as N_{inj} is increased and it becomes small, i.e. $\leqslant$20%, at $N_{inj} \geqslant 1 \times 10^{23}$ [3]. In view of the difficulties encountered in present tokamaks to reach n_c, and of the limitations on the maximum allowed amount of injected gas, imposed by the capabilities of the ITER vacuum pumping and gas exhaust processing systems, the idea of mitigating TQ and suppressing RE simultaneously, with material injection before the TQ, has been abandoned [2].

The ITER DMS is now designed to consist of several material injectors, for gas and/or cryogenic pellets, which can be fired independently. A first set of injectors should provide the plasma with enough impurities to radiate most of the thermal energy during the pre-TQ and TQ, and force the current decay time to within a 50–150 ms interval; the required gas quantity is 2–3 orders of magnitude smaller than necessary to suppress REs through n_c. A second set of injectors will be devoted to suppress/control the RE beam. Crucial for the definition of the RE suppression/control scheme are relatively recent RE experiments, which show that a moderate amount of medium-high Z noble gas clearly causes or accelerates the decay of a RE beam in middle size tokamaks, such as DIII-D ([5] and references within) and AUG (this paper).

3. Forces and thermal quench mitigation

3.1. Experimental conditions and diagnostics

During the 2015–2016 experimental campaign, MGI experiments on AUG were dedicated to explore the effect of small quantities of injected neon, i.e. $N_{inj} = 10^{20}$–10^{22} atoms, on the evolution of the mitigated shut down. A series of target plasmas, without disruption precursors, and with different values of thermal energy, $E_{th} = 30$–750 kJ, were shut down by decreasing amounts of neon, in order to document any variation of the energy deposited onto the divertor and the associated change of fraction of radiated energy (section 3.4). Other relevant plasma parameters were: plasma current $I_p = 1$ MA, magnetic energy $E_{mag} \equiv LI_p^2/2 \simeq 1.4$ MJ (L is the plasma self-inductance), magnetic field $B_t \sim -2.5$ T and safety factor $q_{95} \sim 4.3$. Reproducible disruptive scenarios with a medium-large target thermal energy (e.g. beta limit) are not available for AUG, since tearing modes typically deteriorate the thermal confinement and reduce the thermal energy before the TQ.

An additional series of ohmic plasmas ($I_p = 1$ MA and $q_{95} = 3.5$), in which tearing modes were created by driving the plasma to the density limit and the $n = 1$ component of the MHD modes was, on a shot-to-shot basis, locked at different toroidal angles by the RMP (resonant magnetic perturbation) coils, was terminated by circa 2×10^{21} neon atoms. The toroidal angle between the injection location and the position of the $n = 1$ X point was scanned, in order to investigate its influence on the toroidal asymmetry of the radiated power (section 3.5).

The experiments were performed with one or two in-vessel valves described in [3]. The two valves are located on the low field side of the torus, in two toroidally opposite sectors (sector 13 and 4, see figure 1). They have gas reservoir volumes of 80 and 85 cm^3 and nozzle diameters of 13 and 14 mm respectively, an opening time $<$1 ms and a maximum reservoir pressure of 50 bar. The diagnostics relevant for the work presented in this article are shown in figure 1 and will be introduced along with the discussion of the related measurements.

3.2. Pre-thermal quench phase

3.2.1. Experimental observations. The pre-TQ phase is the time interval between the arrival of the first impurity gas at the plasma edge and the start of the TQ. Its duration, Δt_{pre-TQ}, is

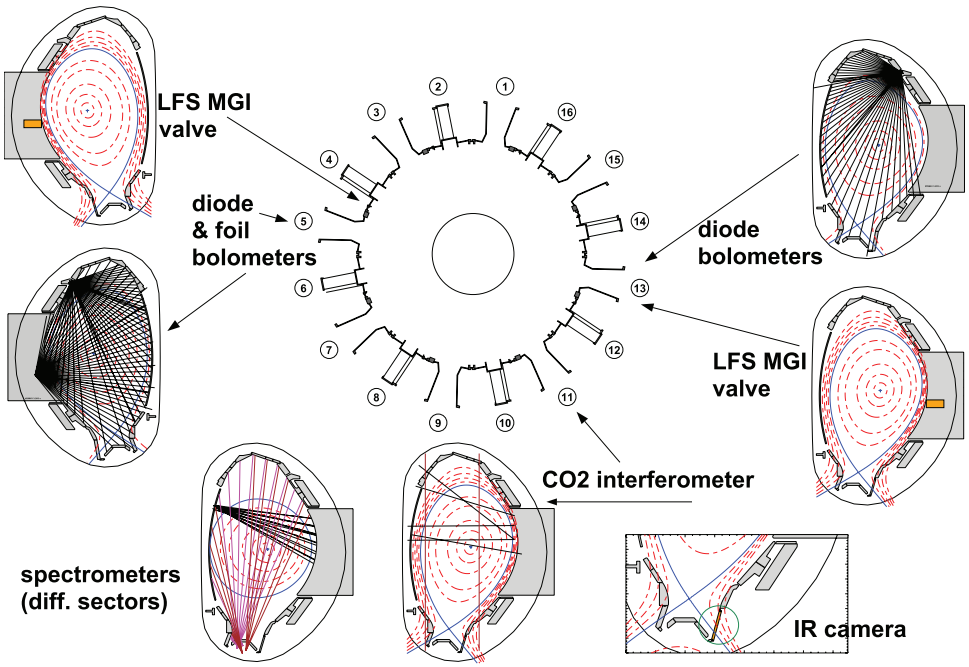

Figure 1. Overview of AUG diagnostics relevant for disruption studies.

an important parameter because it is the amount of gas, which is assimilated in this phase, that radiates part of the thermal energy before the TQ, and determines the initial current decay rate and eventually the RE generation rate. Experimentally (see figure 2), it is found that over a wide range of neon $N_{\rm inj}$, going from 10^{21} to 10^{23} atoms in AUG, $\Delta t_{\rm pre-TQ}$ decreases only by a factor of 2. Nevertheless, decreasing $N_{\rm inj}$ below 10^{21} neon atoms causes a rapid variation of the disruption evolution. In particular, it causes a rapid increase of $\Delta t_{\rm pre-TQ}$, of one order of magnitude when decreasing $N_{\rm inj}$ from 10^{21} to 2×10^{20}. Not only the TQ occurs later, but the discharge starts suffering from minor disruptions, which can cause the loss of vertical stability of a plasma at full current.

$\Delta t_{\rm pre-TQ}$ is found to vary within a factor of two in the set of discharges with locked mode, used to study the radiation asymmetry, but to be, on average, of the same magnitude as in discharges without a locked mode. This is different (for reasons not known) from results published in [3], in which plasmas with large rotating or locked modes were found to be more unstable and exhibit a smaller $\Delta t_{\rm pre-TQ}$.

$\Delta t_{\rm pre-TQ}$ depends very weakly on $E_{\rm th}$ over the whole $N_{\rm inj}$ range explored. This last observation does not have an intuitive explanation and has partly motivated the work of simulation of the pre-TQ phase with the 1D ASTRA-STRAHL code, which is outlined in the following.

3.2.2. Simulation results. The 1D transport code ASTRA, coupled with the 1D radiation code STRAHL and the 2D axisymmetric equilibrium reconstruction code SPIDER, has been used to simulate the pre-TQ phase of MGI induced shutdowns in AUG [4]. Although the fast onset of the TQ, following the interaction of impurities and plasma, is a 3D process, the code ASTRA-STRAHL can reproduce the observed pre-TQ duration and its parametric dependence on several plasma and gas parameters.

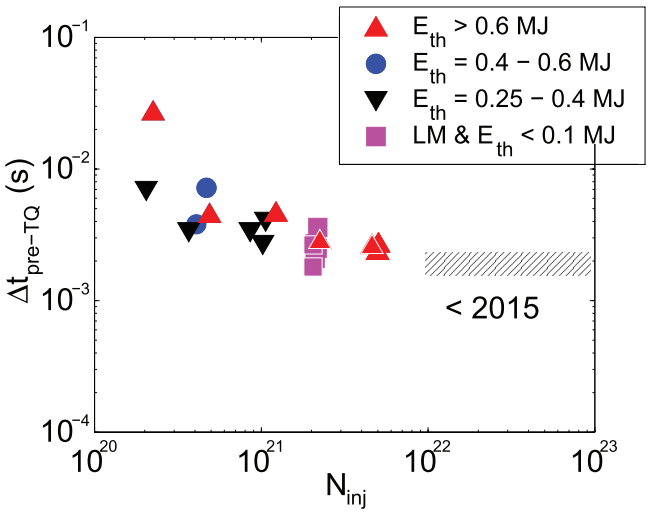

Figure 2. Pre-TQ duration ($\Delta t_{\rm pre-TQ}$) versus the injected number of neon atoms injected ($N_{\rm inj}$) for different ranges of plasma thermal energy ($E_{\rm th}$). The hatched area represents older results published in [3].

The simulations show that the penetration of the neutrals into the plasma is slower than their speed velocity but faster than diffusion. The neutrals rely on the progressive cooling of the plasma, from the edge to the core (and therefore on the radiated power), to penetrate. Therefore the cold front penetration velocity is found to be proportional to the total radiated power. Moreover, the simulations reveal why $\Delta t_{\rm pre-TQ}$ saturates with increasing $N_{\rm inj}$: injecting impurities above a given amount does not accelerate the phase because the gas ionizes in the already cold edge region and does not contribute to the radiated power.

It is postulated that the pre-TQ ends (and the TQ occurs) when the $q = 2$ surface is cooled down and an $m = 2$, $n = 1$ tearing mode grows. This physical picture is supported by

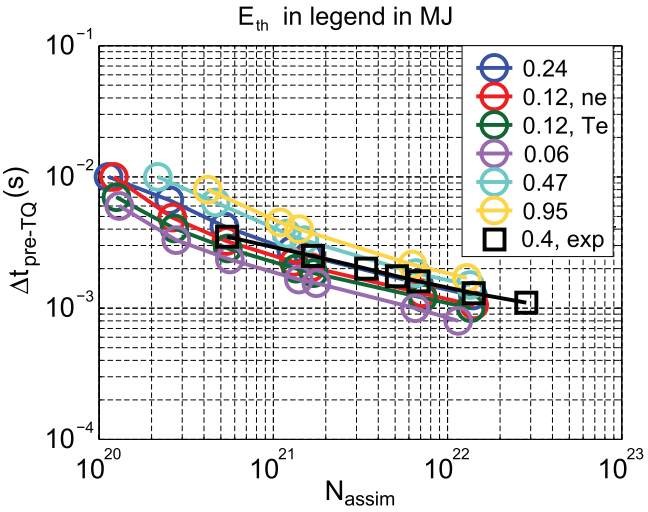

Figure 3. Duration of the pre-TQ phase ($\Delta t_{\mathrm{pre-TQ}}$), simulated by ASTRA-STRAHL, versus the assimilated number of neon atoms (N_{assim}) for different values of the plasma thermal energy (E_{th}), listed in the legend. The 'exp' case has plasma parameter profiles derived from an existing discharge. The other simulations are done on 'artificial plasmas' derived from the existing one by rescaling the density ('ne'), or the temperature ('Te') or both profiles.

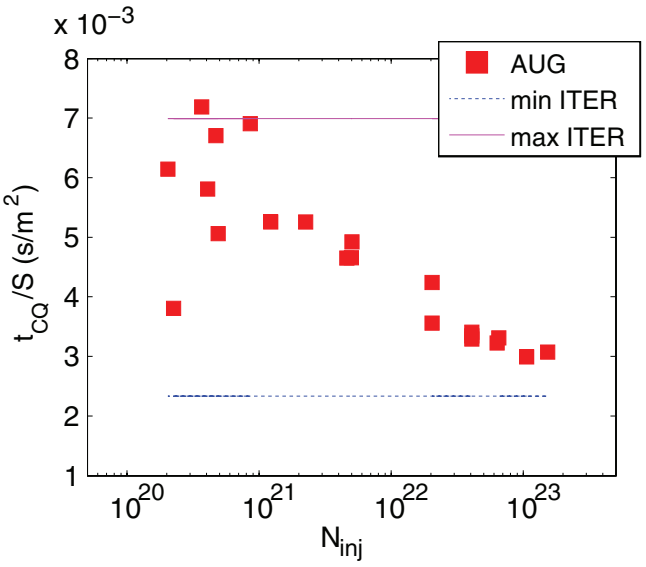

Figure 4. Area-normalized current decay time (t_{CQ}/S) versus the number of injected neon atoms (N_{inj}). The horizontal lines represent the upper and lower boundary of the t_{CQ}/S interval prescribed for ITER.

diode array fast measurements of a cold and radiating front penetration. Accordingly, the pre-TQ phase is defined in the simulations as the time interval necessary for the electron temperature at the $q = 2$ surface to cool to 5 eV.

$\Delta t_{\mathrm{pre-TQ}}$ is plotted in figure 3 versus the injected and completely assimilated (N_{assim}) number of neon atoms, since the code does not simulate particle loss mechanisms. In figure 2 the experimental $\Delta t_{\mathrm{pre-TQ}}$ is shown versus N_{inj}, which is a known quantity; the actual number of assimilated neon atoms is not known in this phase, since the density is toroidally and poloidally asymmetric and density measurements are available only in one sector of AUG. The assimilation fraction is estimated to be in the range 30–50% at $N_{\mathrm{inj}} < 10^{22}$. The assimilation of larger amounts of injected neon is discussed in [3].

3.3. Current quench and mechanical forces

3.3.1. Current quench time. The CQ duration, Δt_{CQ}, is a parameter necessary for the design of the ITER nearby plasma-facing conductive structures, for several reasons:

- along with the plasma vertical movement, Δt_{CQ} determines the magnitude of the induced eddy currents and related mechanical stresses in the first-wall and blanket modules;
- in competition with the growth rate of the plasma vertical displacement, it determines the vertical force on the vessel and other stabilizing components, through halo and induced toroidal currents;
- Δt_{CQ} determines the toroidal electric field, which tends to generate the runaway electrons.

Δt_{CQ} is mainly determined by the power balance $P_{\mathrm{oh}} \simeq -\mathrm{d}E_{\mathrm{mag}}/\mathrm{d}t$ (with P_{oh} being the ohmic power dissipated by the cold plasma). In particular, the area-normalized current decay time, i.e. $\Delta t_{\mathrm{CQ}}/S$ (where S is the area of the plasma poloidal cross section), is a proxi for the plasma resistivity during the CQ and has been used for cross-machine comparison of Δt_{CQ} and extrapolation to ITER. The CQ time in ITER will have to be tailored in the range $\Delta t_{\mathrm{CQ}} = 50$–150 ms [2], or equivalently $\Delta t_{\mathrm{CQ}}/S = 2.3$–7.0 ms m^{-2} (with $S = 21.3$ m^2 being the area of the ITER plasma poloidal cross section) in order to avoid large eddy currents and large vertical forces.

The definition $\Delta t_{\mathrm{CQ}} \equiv (t_{20} - t_{80})/0.6$ [1] is used here, with t_{80} and t_{20} being the times at which the I_{p} has decayed to 80% and 20% of its pre-disruption value respectively.

The minimum value of $\Delta t_{\mathrm{CQ}}/S$ in AUG ($S \simeq 1.2$ m^2) is about 2 ms m^{-2} and is reached in natural disruptions during vertical displacement events (VDEs). As shown in figure 4, the present series of mitigated disruptions has an area-normalized current decay time decreasing with increasing N_{inj} and is within the 'prescribed ITER range'. This result suggests that mitigation of the eddy currents and of the vertical force should be possible in ITER over a wide range of N_{inj}. Only at $N_{\mathrm{inj}} < 4 \times 10^{20}$ does the experimental data approach the upper end of the prescribed Δt_{CQ} ITER range. The scatter of the data-points at these lower values of injected gas (figure 4) is due to the appearance of minor disruptions, which can induce a VDE and a short CQ, caused by the cooling effect of the strong interaction divertor-plasma and not by MGI.

3.3.2. Halo current and vertical force on the vessel. The total vertical force on the AUG vessel is the sum of the forces generated by the halo currents, flowing mostly poloidally in the vessel between the inner and outer divertor plates, by the toroidal current induced in the passive stabilizing loop (PSL) and by the toroidal current flowing in the vessel.

AUG is equipped with shunts for the measurement of halo currents (I_{halo}) in the lower divertor. Halo currents of up to

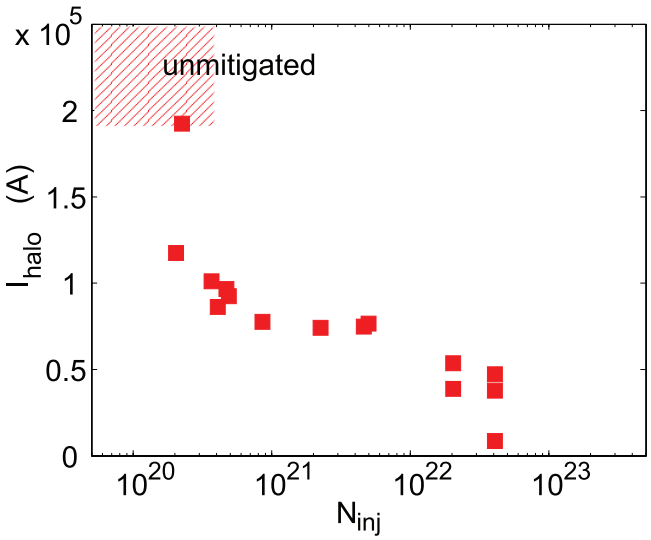

Figure 5. Halo current (I_{halo}) versus the number of injected neon atoms (N_{inj}).

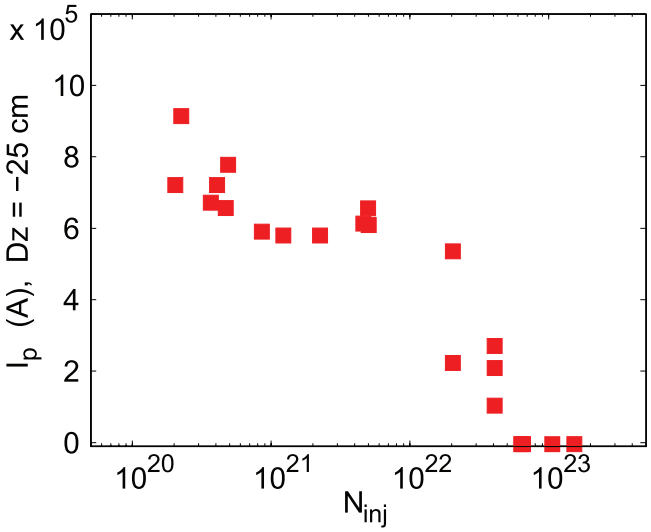

Figure 6. Toroidal current (I_p), carried by the plasma which underwent a vertical displacement (Dz) of 25 cm, versus the number of injected neon atoms (N_{inj}).

40% of the pre-disruption plasma current have been observed in unmitigated disruptions. Impurity injection reduces the maximum halo current because it accelerates the toroidal current decay after the TQ and prevents the formation of a halo region carrying a large parallel (to the magnetic field lines) current. The reduction of I_{halo} following the increase of N_{inj} is shown in figure 5. Its monotonic but steplike behavior can be understood from figure 6. This figure shows the value of the current of the plasma at the time it has moved vertically (towards the lower divertor in these cases) by 25 cm from the pre-disruption position. These plasmas had an initial $I_p \sim 1$ MA. For $N_{inj} \leqslant 10^{21}$, approximately 40% of I_p has decayed while the plasma has moved of 25 cm. For $N_{inj} > 3 \times 10^{22}$ the CQ occurs while the plasma is still centred in the machine, because the CQ becomes faster than the vertical displacement.

AUG is also equipped with strain gauges on the vessel suspension rods: these record a total vertical force, F_{vv}, in the

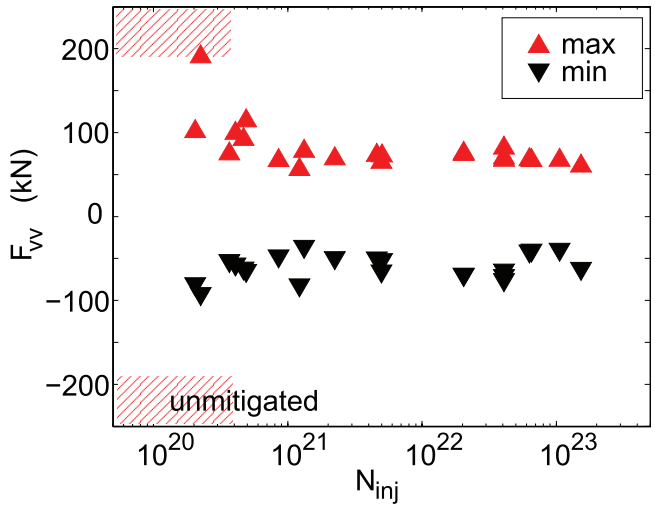

Figure 7. Maximum (max) and minimum (min) vertical force on the vacuum vessel (F_{vv}), measured by strain gauges, versus the number of injected neon atoms (N_{inj}).

range $-100 \div 100$ kN for $N_{inj} > 10^{21}$, increasing in absolute value as the neon amount is reduced. The vacuum vessel oscillates after the disruption and figure 7 shows the maximum and the minimum F_{vv} values reached as N_{inj} varies. In past unmitigated disruptions, $|F_{vv}/I_p|$ has reached 600 kN MA^{-1} (see figure 22 of [6]).

The vertical force acting on the PSL, which is a significant component of F_{vv}, is presently not measured and therefore not discussed here.

A reduction of the mechanical forces following MGI in AUG cannot be extrapolated to ITER without self consistent modeling of the whole plasma-conductor interaction. Therefore the benchmark and model development of appropriate numerical codes (e.g. TSC [7] and DINA [8]) is an ongoing activity within the ITPA MHD topical group [19].

3.4. Thermal loads

One of the purposes of the work presented here is to document the influence of N_{inj} on the repartition of the plasma energy dissipated during a disruption: in fact, it is to be feared that a reduction of the injected impurity amount could result in a reduction of the fraction of the radiated power and into an increment of the fraction conducted onto the divertor plates.

AUG is equipped with several foil-bolometers, located in one toroidal sector (figure 1), measuring the radiated power with a time resolution of one ms. Diode-bolometers, located in two toroidal sectors 180° apart, allow for finer time resolved measurements of photon emission during the pre-TQ and the TQ; nevertheless they must be calibrated by comparison with the foil bolometers.

The power deposited on a small area (20×1 cm^2) of the outer divertor (P_{div}), about the strike point of the target plasma separatrix has been measured every 0.4 ms (following a trade-off between time resolution and area) by an infra-red camera. The foot-print of the heat flux onto the divertor is localized within the viewed area during the pre-TQ. However, during

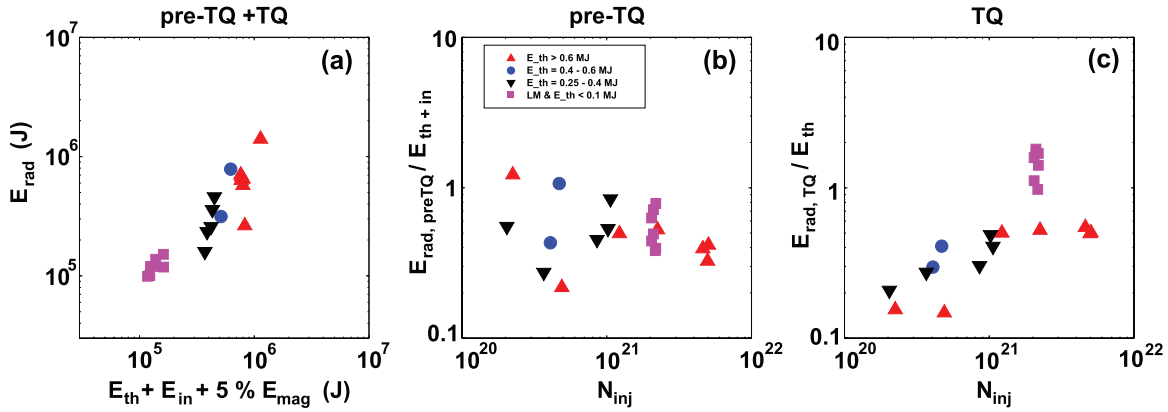

Figure 8. (a) Energy radiated during the pre-TQ and TQ phases (E_{rad}) versus the energy available for dissipation, i.e. the sum of the target thermal energy (E_{th}), of the auxiliary energy in input (E_{in}) and 5% of the magnetic energy (E_{mag}). (b) $E_{rad}/(E_{th} + E_{in})$ versus N_{inj} during the pre-TQ. (c) E_{rad}/E_{th} versus N_{inj} during the TQ.

the TQ, the heat flux onto the divertor is deposited on a poloidally broader surface; nevertheless localized measurements can still be significant.

The energy radiated (E_{rad}) during the whole pre-TQ and TQ phase is plotted on figure 8(a) versus the energy available for dissipation during this phase. E_{rad} is measured by the diode-bolometers and averaged over the two toroidal sectors. The available energy is defined to be $(E_{th} + 5\% \times E_{mag} + E_{in})$, with E_{in} being the total auxiliary power. This figure indicates that the amount of energy available for dissipation is mostly radiated and found as E_{rad}, independent of E_{th} or N_{inj}: therefore a decrease in N_{inj} does not clearly result into a decrease of E_{rad}. The fraction of '5%' is a somehow arbitrary small fraction of E_{mag}. Thus, figure 8(c) (and later figure 9 as well) shows that plasmas with low E_{th} dissipate (i.e. radiated and conduct onto the divertor) a fraction of their thermal energy larger than the plasmas with larger E_{th}. This suggests the hypothesis that a fraction of E_{mag} is also dissipated during pre-TQ and TQ.

No clear trend of E_{rad}/E_{th} is seen during the pre-TQ phase (figure 8(b)).

E_{rad}/E_{th} does decrease with N_{inj}, independently of E_{th}, during the TQ (figure 8(c)); the TQ is defined as the 1 ms time interval about the maximum value of P_{rad}. Nevertheless, this tendency is due, in several discharges, to a larger fraction of E_{th} being radiated during the pre-TQ (figure 8(b)), because the plasma is longer stable or it undergoes several minor disruptions (only one of them is considered as TQ), and therefore to a smaller E_{th} available before the TQ.

The data points at $N_{inj} \sim 2 \times 10^{21}$, rising above the others on figure 8(c), pertain to target plasmas with a very low E_{th} (<0.1 MJ). E_{rad}/E_{th} is larger than unity in these cases probably because a fraction of E_{mag} is also being radiated. The same explanation could apply to this set of data points in figure 9.

The hypothesis that the ratio of conducted to radiated energy increases in the pre-TQ and in the TQ, when less gas is injected, is not confirmed for all cases by the bolometric measurements. However, the thermography measurements indicate that a larger fraction of thermal energy can be deposited in the divertor during the TQ. Figure 9 shows two branches of E_{div}/E_{th} at low N_{inj}: the upper data points pertain to TQs, which consist of one single (radiated and deposited)

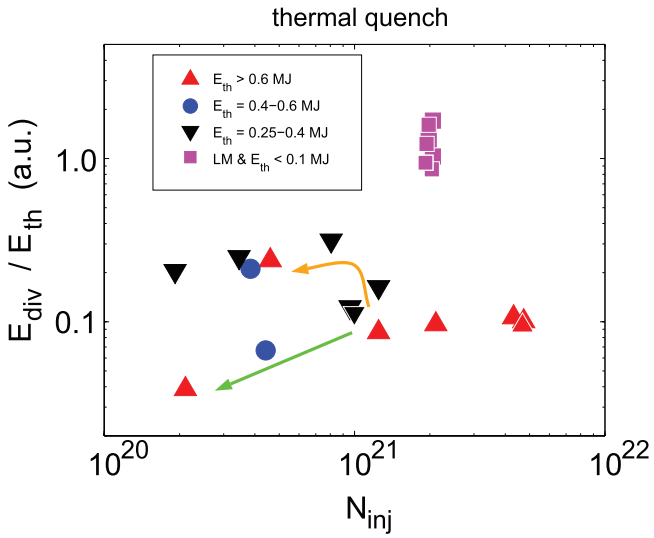

Figure 9. Energy deposited on a limited area of the outer divertor (E_{div}) during the thermal quench (TQ), normalized to the target thermal energy (E_{th}).

energy spike, while the plasmas of the lower set lose energy with a sequence of bursts. E_{div} in this figure is defined as the energy measured on the mentioned divertor area during 1 ms about the maximum P_{div}.

In AUG, thermography measurements suggest that $N_{inj} > 10^{21}$, with $N_{assim} \simeq 0.3$–$0.4 \times N_{inj}$, are required to ensure thermal load mitigation on the divertor plates. ASTRA-ZIMPUR simulations, presented in [9], indicate that $N_{assim} > 2 \times 10^{22}$ of neon are necessary to mitigate an ITER TQ. JET results presented in [10] show a decrease of the fraction of the radiated power over the whole disruption at $N < 4 \times 10^{21}$ of neon injected before the TQ in a mixture of 90% D_2 and 10% Ne. These numbers suggest that, the neon amounts necessary for heat load mitigation in AUG, JET and ITER scale roughly with the plasma volume, i.e. V_{AUG}:V_{JET}:V_{ITER} = 13:100:840 m^3.

At this point we can conclude that the minimum quantity of assimilated gas, necessary for the mitigation of the thermal load and of the mechanical forces in ITER, and how it will depend on the use of either pellets or gas, must still be confirmed by

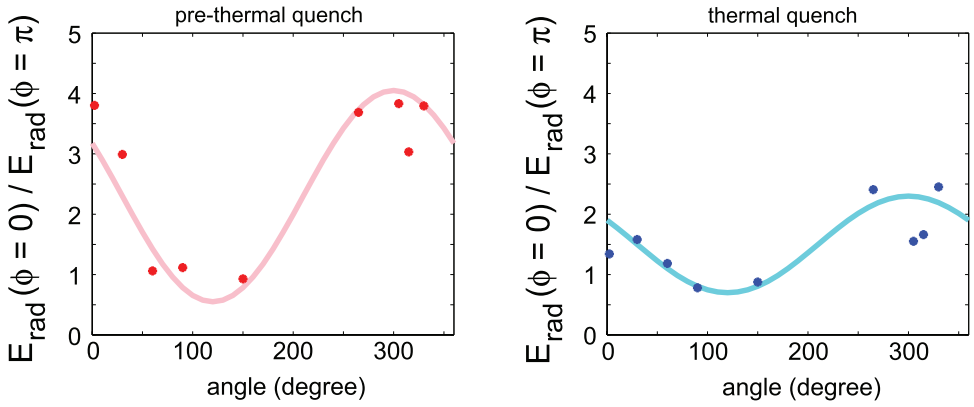

Figure 10. Ratio between the energy radiated in front of the gas injection location ($E_{\rm rad}(\phi = 0)$) and the energy radiated in the sector 180 degree apart ($E_{\rm rad}(\phi = \pi)$) during the pre- thermal quench (left) and thermal quench (right) versus position of the maximum $n = 1$ component of the radial magnetic field, as measured by the saddle coils on the HFS.

further experiments and extrapolation through modelling. The 3D nature of the energy flow and radiative dissipation (following section), the large surface area (extending to the whole divertor surface and beyond) affected by the energy deposition, the limited surface area monitored by the diagnostics and the errors affecting the measurements are some of the reasons why the treatment of this problem is never conclusive.

3.5. Asymmetric radiation distribution during the pre-TQ

During the pre-TQ, both the injected impurities and the radiated power density, $\mathcal{P}_{\rm rad}$, are strongly poloidally and toroidally asymmetric, and typically larger in the vicinity of the valve. The presence of rotating MHD modes—and probably also the plasma rotation, carrying the impurities toroidally away from the injection location—can reduce the toroidal asymmetry of the energy radiated in this phase. During the TQ, both density and radiation asymmetries decrease, suggesting that a mixing of the impurities in the plasma takes place.

The spatial distribution of the radiated energy is studied in existing tokamaks, motivated by the report in [11] that an increase of a factor of two in the energy deposited on the wall with respect to the energy assumed uniformly radiated during an ITER pre-TQ ($E_{\rm th} = 350$ kJ within 1 ms) would melt the Be wall.

A key reference for the interpretation of the radiation asymmetry after MGI is [12]: simulations performed with NIMROD pointed out that the relative position of valve, with respect to the $n = 1$ X point, strongly influences the magnitude of the asymmetry; in particular, the maximum $\mathcal{P}_{\rm rad}$ occurs when the impurities are injected into the X point of the $n = 1$ existing modes.

Ohmic plasmas, with tearing modes induced by density limit, were used to document the variation of radiation asymmetry (see also section 3.1). The modes, with a typically dominant $n = 1$ toroidal number, were intentionally locked by a resonant $n = 1$ magnetic field created by the RMP coils at different toroidal positions. Neon injection into the plasmas was triggered by the locked mode trigger, once the amplitude of $n = 1$ component of the radial magnetic field ($\tilde{B}_{r,n=1}$) exceeded a given threshold.

The magnitude of the ratio of the energies radiated in two toroidally opposite sectors (the valve is positioned at $\Phi = 0$), $E_{\rm rad}(\Phi = 0)/E_{\rm rad}(\Phi = \pi)$, reaches the maximum values of 4 and 2.5 during the pre-TQ and during the TQ respectively. This ratio exhibits a sinusoidal curve, as shown in figure 10 versus the position of the maximum $\tilde{B}_{r,n=1}$, as measured by the saddle coils on the HFS.

The effect of rotation on the asymmetry is suppressed and the effect of toroidal spreading of the impurities—due to parallel thermal velocity—is limited by the low plasma temperature in this dedicated experiment. This data-set is particularly suited for the benchmark of 3D non-linear MHD codes, such as JOREK, which is being further developed for disruption modelling [13]. In previous experiments [14], it was found that plasmas at larger energies could not be stopped by the RMPs and therefore the radiation asymmetry was affected by a, difficult to measure, residual rotation.

4. Generation and dissipation of REs

4.1. Background

Runaway electrons (REs) are expected to be generated in ITER disruptions at full plasma current [2]. While the generation mechanisms of REs are relatively well understood, there is no general consensus on which loss mechanisms are dominant in present experiments, and which will prevail in ITER. This makes the calculation of the expected RE current and energy—and the consequent damage to the plasma facing components—uncertain and the design of the ITER disruption mitigation system challenging.

AUG disruptions, typically of diverted and elongated plasmas, do not exhibit formation of RE beams for the following reasons: usually, a disrupting plasma has a density large enough to suppress the Dreicer generation; the avalanche generation is not expected to be significant in AUG; during the current quench, an elongated plasma becomes vertically unstable, moves up- or downwards, becomes limited on the lower or upper divertor and develops a halo, i.e. a region of open flux surfaces from which the REs escape, within milliseconds. Therefore, in order to allow studies of RE generation

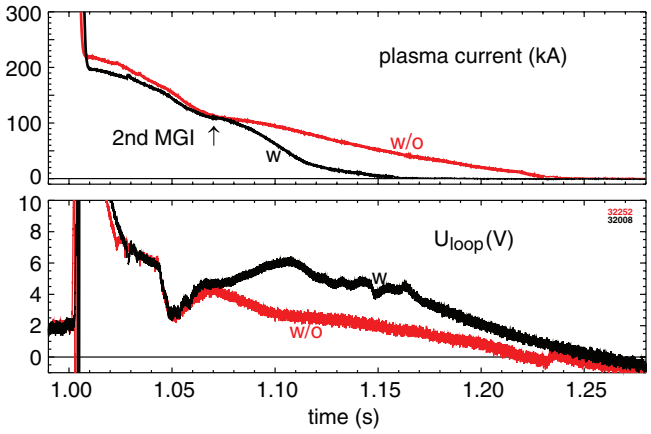

Figure 11. Time traces of the plasma current (above) and of the loop voltage measurements (below) for RE beams with (w) and without (w/o) second argon injection at 1.07 s.

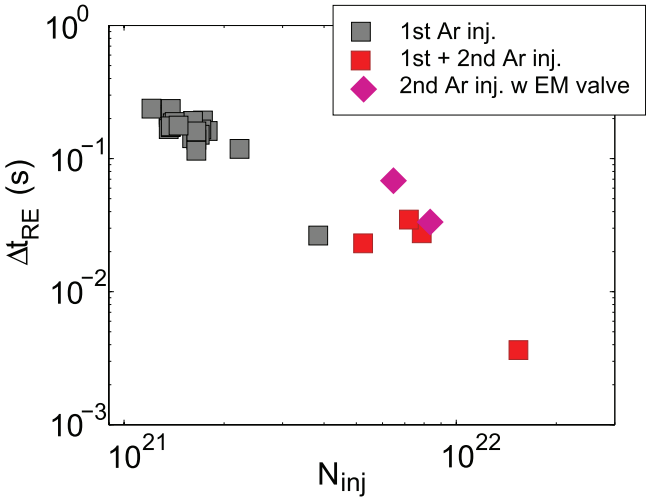

Figure 12. Life time of RE beam (Δt_{RE}) versus the total (i.e. 1st + 2nd) injection, amount of argon injected (N_{inj}).

and dissipation during disruptions, a scenario for RE generation during the TQ had to be—and was—established during the 2014 campaign [15], and further extended and explored in 2015. The main aim of the 2015 experiments was to explore the possibility of influencing the RE generation and losses within the range of variability of machine and plasma parameters. This paper concentrates on one aspect of the available analysis, namely on the RE current suppression by argon MGI and the evaluation of the friction force on the REs.

4.2. Experimental scenario and measurements

REs have been generated by injecting 1.7–5 $\times 10^{21}$ atoms of argon in a low target density (volume averaged $n_e < 2{-}3 \times 10^{19}$ m^{-3}) circular limiter plasma, with $I_p \sim 0.8$ MA, $B_t \sim -2.5$ T, $q_{95} \sim 4$ and 2–2.5 MW of ECRH heating. The injected argon induces a fast quench of the current carried by thermal electrons, followed by a long-lived runaway beam, forming a toroidal current of up to 400 kA, and lasting up to 500 ms. The RE beam current and duration are found to be reproducible. Nevertheless, changes in the current ramp up history influence the RE current/duration, supposedly because of changes in the current profile and the resulting MHD activity before and during the TQ.

Changes in the toroidal magnetic field and therefore in the safety factor, in the deposited ECRH power and deposition location, in the heating and current drive scheme, in the reference current imposed by the control system, and the application of RMPs were also undertaken. These studies must be further exploited and extended; therefore, the related experimental results will not be discussed in this article.

The circular plasma carrying the RE beam is vertically stable. The plasma position and the shape, deduced from equilibrium reconstruction, are in agreement with soft x-ray profiles. The plasma control system does not contribute to the beam vertical stability because the current in the control coils is for part or all of the time saturated. A slow vertical displacement of the RE beam sets-in only in a few cases and does not affect the overall RE current decay rate.

The plasma-RE current is controlled by the control system. After injection of small amounts of argon, i.e. $\leqslant 2 \times 10^{21}$ atoms, the controlled current follows the pre-programmed waveform; larger amounts of argon increase the RE losses, accelerate the current decay with the result that the OH system cannot keep the actual current at the level of the reference value.

Line integrated measurements of the electron density, n_e, are available during the whole RE beam lifetime from 5 DCN interferometer chords and from 2 CO_2 chords. The n_e profiles could be reconstructed for all the discharges during most of the RE beam because a magnetic equilibrium is available.

The foil bolometers measure a total radiated energy of the order of magnitude of the initial kinetic and magnetic energy of the RE beam. This suggests that radiation plays a significant role in the RE energy dissipation. Measurements of Bremsstrahlung are not available for this dedicated experiment. Synchrotron radiation spectra were recorded with a system developed at ENEA-Frascati and similar to the one used on FTU [16].

Time-resolved measurements of gamma spectra from a gamma/neutron spectrometer are available and can give indication of the RE energy spectra, if interpreted with a model of RE-matter interaction. The reconstruction of the energy distribution function from these measurements is in progress.

4.3. RE suppression

4.3.1. Experimental results. In some of the RE beams generated, argon was injected a second time (0.17 and 0.7 bar $\times$ litre with a second valve) with a delay of 70 ms from the first argon puff (see figure 11. Both an in-vessel valve, with the nozzle some 10 cm far away from the plasma edge, and an electromagnetic valve, 1.5 m far away, were used. The RE current life time, Δt_{RE}, after both the first and the second argon puff, show a clear dependence on the argon amount injected—i.e. the more gas the faster the decay—as illustrated in figure 12. The RE current does not exhibit a regular monotonic decay but rather a 'bumpy' time behavior; therefore Δt_{RE} is here simply defined as

$$\Delta t_{RE} \equiv (t_{end} - t_0)/(I_{RE,end} + I_{RE,0})/2/(I_{RE,0} - I_{RE,end}) \quad (1)$$

The final phase of the current is often characterized by a faster loss of 30–100 kA, followed again by the slower decay of the residual current, <30 kA. Δt_{RE} is evaluated by taking $I_{\mathrm{RE,end}} = 30$ kA for all discharges. $I_{\mathrm{RE},0}$ is the RE current after the 1st or 2nd argon injection, at time t_0.

Figure 12 suggests that RE collisions with the electrons and the high Z impurity atoms is a significant RE current dissipation mechanism. In the following section, the values of collisional damping inferred from current decay and calculated from density measurements are discussed.

4.3.2. RE collisional damping. REs lose energy through different known mechanisms: by inelastic collisions mainly with bound and free electrons, through small angle scattering and transfer of energy to the matter in which they travel; by collisions with ions and Bremsstrahlung radiation; and by cyclotron and synchrotron radiation. The first mechanism, i.e. the friction force of the electrons on the REs, is discussed in this contribution, since the loss of energy by the other mechanisms has not been evaluated yet (although they are believed to be smaller). The correct modelling of the evolution of the RE population requires kinetic calculations. Nevertheless, at least formally, the RE current time evolution (with time constant τ_{RE}) is expected to be described by

$$\frac{1}{\tau_{\mathrm{RE}}} \equiv \frac{\mathrm{d}I_{\mathrm{RE}}}{\mathrm{d}t}\frac{1}{I_{\mathrm{RE}}} = \frac{\mathrm{d}n_{\mathrm{RE}}}{\mathrm{d}t}\frac{1}{n_{\mathrm{RE}}} \simeq \frac{e(E_\phi - E_{\mathrm{c}})}{p_{\mathrm{RE}}} \qquad (2)$$

where E_ϕ is the toroidal electric field, E_{c} is the so-called critical electric field, n_{RE} is the RE density and p_{RE} is the average RE momentum.

In the remaining of this section:

- E_ϕ is calculated from the loop voltage measurement;
- the argon concentration is determined from spectrometric measurement;
- the magnitude of E_{c} is determined by the argon and by the free electron densities;
- a comparison of E_{c} with the measured E_ϕ allows discussing the role of the friction force, i.e. eE_{c}, in the decay of the RE beam.

Toroidal electric field. The evaluation of E_ϕ in the plasma requires a self consistent modelling of the plasma current evolution, which is mainly carried by the REs in the analysed discharges. Numerical modelling is not yet available and therefore the time evolution of the E_ϕ profile in the plasma in not known. Nevertheless, measurements of the loop voltage (U_{loop}) at different poloidal positions around the plasma are available (see figure 11). The closest—to the plasma—U_{loop} coil is inside the vessel, behind the inboard heat shield, some 10 cm distant from the the plasma surface.

An average E_ϕ can also be calculated knowing the plasma self-inductance and the multual-inductance between the plasma and other coils/structures:

$$2\pi R_{\mathrm{c}} E_\phi \simeq L_{\mathrm{p}}\frac{\mathrm{d}I_{\mathrm{p}}}{\mathrm{d}t} + M_{\mathrm{OH-p}}\frac{\mathrm{d}I_{\mathrm{OH}}}{\mathrm{d}t} + M_{\mathrm{vv-p}}\frac{\mathrm{d}I_{\mathrm{vv}}}{\mathrm{d}t} \qquad (3)$$

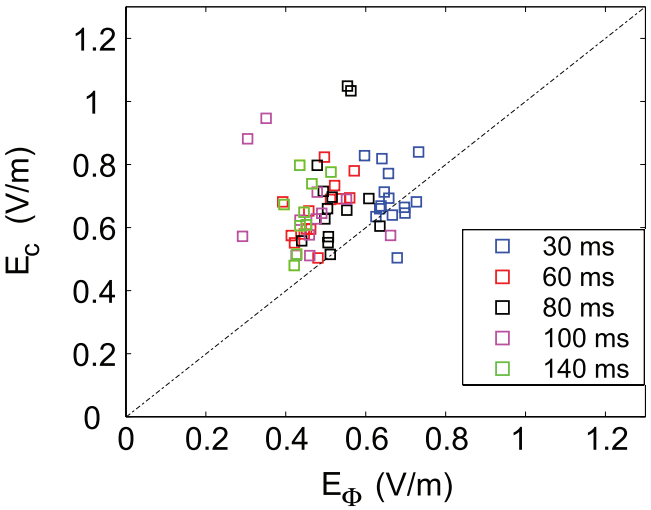

Figure 13. Critical electric field (E_{c}) versus the toroidal electric field (E_Φ) at different times during the RE beam.

where $M_{\mathrm{OH-p}}$ and $M_{\mathrm{vv-p}}$ are the mutual inductances between the OH coils and the plasma, and between the vessel structures and the plasma, respectively. The U_{loop} measurements and the estimations with equation (2) give the following consistent picture: during the CQ, transient U_{loop} values of 40–50 V are reached; during the RE plateau, the loop voltage decreases from 10 to a few V in all cases; during the fast RE termination caused by the second argon injection, transient U_{loop} up to 10 V are generated. $E_\phi = U_{\mathrm{loop}}/(2\pi R_{\mathrm{c}}) \sim U_{\mathrm{loop}}/10\,\mathrm{V\,m^{-1}}$, with a current major radius, $R_{\mathrm{c}} \sim 1.6$ m.

Critical electric field. E_{c} is a linear function of the free and bound electron density; therefore its estimation requires knowledge of the plasma atomic species and their ionization state:

$$E_{\mathrm{c}} = e^3 n_{\mathrm{e,eff}} \ln(\Lambda_{\mathrm{e,free}})/(4\pi\epsilon^2 m_{\mathrm{e}} c^2),$$
$$n_{\mathrm{e,eff}} \equiv n_{\mathrm{e,free}} + \frac{\ln(\Lambda_{\mathrm{e,bound}})}{\ln(\Lambda_{\mathrm{e,free}})} n_{\mathrm{e,bound}} \qquad (4)$$

The symbols used in the previous equation have the following meaning: e is the electron charge, $n_{\mathrm{e,eff}}$ is an effective electron density, sum of the free electron density, $n_{\mathrm{e,free}}$ and of the bound electron density, $n_{\mathrm{e,bound}}$, multiplied by a factor; this factor is the ratio between the Coulomb logarithm for bound-free electron collisions and the Coulomb logarithm for free–free electron collisions. Impurities other than argon are neglected here.

Argon concentration. Several spectrometers were configured to record line emission from Ar-I, Ar-II, C-II and C-III during the RE beam. The line integrated measurements of light emitted by specific transitions allow a spatially resolved calculation of the argon and carbon densities and of the electron temperature (T_{e}) once the free electron density is known, since the line radiance, L, is given by the following integral along the line of sight:

$$L = \frac{1}{4\pi} \int n_e \, n_z \, f_z \, X_{eff} \, dl \quad (5)$$

The photon emissivity coefficients, X_{eff}, for the relevant transitions have been calculated from a collisional radiative model. The model considers only the population of the higher states by electron excitation collisions; for the solution of the collisional radiative model, the ADAS208-code [17] has been used. The fractional abundances of carbon and argon, f_z, have been calculated from the ADAS data sets for rate coefficients of ionization and recombination, assuming a balance of ionization and recombination rates. An additional data set, derived from data available in [18], were also computed and show a somewhat different ratio f_{Ar-I}/f_{Ar-II}.

The comparison between the line integrated emission of C-II and C-III and the respective (f_z X_{eff}) factors suggests $T_e \leqslant 1.8$ eV. At this temperature the argon and carbon are expected to be mostly singly ionized. Indeed, the measurements of C-III are at or below the noise level, indicating no significant concentration of this carbon ionization state; Ar-I is also clearly present over the whole plasma. Together, both observations suggest a $T_e < 2$ eV. The comparison between the line integrated emission of Ar-I and Ar-II and the calculated (f_z X_{eff}) factors is not conclusive, since the two sets of f_z suggest rather different T_e values.

With the uncertainties just discussed, an argon concentration of around 100% is derived from equation (5) using the measurements of Ar-II radiation for the specific discharges analyzed. This order of magnitude is consistent with the ratio of 10:1 between the quantities of argon and deuterium injected in one discharge.

Critical versus toroidal electric field. Figure 13 summarizes the comparison between the measured E_ϕ and E_c induced from the argon density estimates and n_e measurements (at different times after the CQ). The critical electric field is typically larger than the toroidal electric field sustaining the RE beam, and therefore significantly accounts for the RE energy losses associated with the observed current decay.

Although large error bars affect the estimated argon concentration and thus of E_c—because of uncertain radiation coefficients—we can conclude that the plasma composition of the AUG RE beams is different from the one obtained at DIII-D. There, the RE beams have a smaller argon concentration [5] and anomalous RE current dissipation mechanisms, one order of magnitude more efficient than e-RE collisions, have to be invoked to explain the observed RE current decay rate. The AUG result does not exclude a significant role of the RE-ion collisions in the decay of the RE current or the presence of other loss mechanisms; nevertheless these mechanisms would have an effect quantitatively comparable to the effect of the e-RE collisions.

5. Summary

The range of neon quantities injected in AUG plasmas during MGI experiments has been extended below the minimum quantity necessary for disruption mitigation and the influence of these quantities on the induced plasma-shutdown have been analyzed and documented.

1D modelling of the pre-TQ phase, performed with the code ASTRA-STRAHL, reproduces its duration and the parametric dependences observed experimentally. The code can therefore be used to determine ITER pre-TQ. The cooling of the $q = 2$ surface below 5 eV is a good criteria for the TQ onset.

The observed normalized CQ duration is in the prescribed ITER range over a wide range of N_{inj} values. Forces and heat load are mitigated in AUG with $N_{inj} > 10^{21}$ atoms of neon. At lower quantities of gas the forces increase towards the unmitigated values.

Thermography data provide experimental indication that more energy is deposited onto the divertor plates during the TQ as the gas amount is decreased. Nevertheless, the problem of characterizing the thermal loads during disruptions has been and remains complex because of the 3D nature of the energy flow and of the radiative dissipation.

A scenario for the generation of runaway electrons during the CQ has been established by injecting small quantities of argon into a low density target plasma and it allows for the study of runaway formation and losses. The main finding is that the quantity of argon injected, to create and then suppress the REs, has a clear influence on the time decay of the RE beam, i.e. the more impurities, the faster the RE current decay. The critical electric field, calculated from the electron density and the concentration of argon, is larger than the toroidal electric field sustaining the RE beam, and thus significantly accounts for the RE energy losses associated with the observed current decay. Large error bars affect the estimated argon concentration because of uncertainties in the radiation coefficients. Quality atomic data for argon (or other high-Z impurity used to dissipate the RE beam) at low temperatures are essential for the understanding of the whole problem of RE losses.

Acknowledgments

The first author acknowledges useful discussions with Michael Lehnen (IO). This work has been carried out within the framework of the EUROfusion Consortium and has received funding from the Euratom research and training programme 2014–2018 under grant agreement No 633053. The views and opinions expressed herein do not necessarily reflect those of the European Commission.

References

[1] Hender T C *et al* 2007 *Nucl. Fusion* **47** 128–202
[2] Lehnen M *et al* 2015 *J. Nucl. Mater.* **463** 39
[3] Pautasso G *et al* 2015 *Nucl. Fusion* **55** 033015
[4] Fable E *et al* 2016 *Nucl. Fusion* **56** 026012
[5] Hollmann E M *et al* 2015 *Phys. Plasma* **22** 021802
[6] Pautasso G *et al* 2007 *Nucl. Fusion* **47** 900–13
[7] Bandyopadhyay L *et al* 2016 *Plasma Disruption, VDE Modelling in Support of ITER, TH/P1-19 and IAEA Conf. (Kyoto, Japan, 17–22 October 2016)*
[8] Miyamoto S *et al* 2014 *Nucl. Fusion* **54** 083002

[9] Leonov V *et al* 2011 *38th EPS Conf. on Plasma Physics Strasbourg (France)* (contribution P2.108)
[10] Jachmich S 2016 Disruption mitigation at JET using massive gas injection *43rd EPS Conf. on Plasma Physics Leuven (Belgium)*
[11] Sugihara M *et al* 2007 *Nucl. Fusion* **47** 337
[12] Izzo V *et al* 2013 *Phys. Plasmas* **20** 056107
[13] Nardon E *et al* 2016 Progress in understanding disruptions triggered by massive gas injection via 3D non-linear MHD modelling with JOREK *43rd EPS Conf. on Plasma Physics (Leuven, Belgium)*
[14] Pautasso G *et al* 2013 MGI in plasmas with locked modes *Proc. 40th European Physical Society Conference on Plasma Physics (Espoo, Finland)* paper O5.104
[15] Pautasso G *et al* 2015 Generation and suppression of runaway electrons in ASDEX Upgrade disruptions *42nd EPS Conf. on Plasma Physics (Lisbon, Portugal 22–26 June 2015)*
[16] Esposito B *et al* 2016 Runaway electron generation and control *43rd EPS Conf. on Plasma Physics (Leuven, Belgium)*
[17] Summers H P 2004 ADAS User Manual 2.6 www.adas.ac.uk./manual.php
[18] FLYCHK: generalized population kinetics and spectral model for rapid spectroscopic analysis for all elements 2005 *High Energy Density Physics* vol 1, ed H-K Chung *et al* (Oxford: Elsevier) p 3–1
[19] www.iter.org/org/team/fst/itpa